Ultrahigh-vacuum organic molecular-beam deposition system for *in situ* growth and characterization

Emilia Annese,[a,b]* Joacir E. dos Santos,[a] Gustavo Lorencini M. P. Rodrigues,[a] Andre Silva Rocha,[a] Horacio Ribeiro de Moraes[a] and Julio Criginski Cezar[a]

[a]Laboratório Nacional de Luz Síncrotron – Centro Nacional de Pesquisa em Energia e Materiais – CP 6192, 13083-970 Campinas, SP, Brazil, and [b]Programa Engenharia Química, COPPE, Universidade Federal de Rio de Janeiro, Rio de Janeiro, Brazil. *Correspondence e-mail: emiliaannese@gmail.com

A compact ultrahigh-vacuum molecular-beam deposition system has been developed for the *in situ* synthesis of organic thin films and multilayers. The system incorporates all the features (heater, thickness monitor, evaporators) necessary for controlled organic thin-film growth. It can be used independently, or it can be docked to the *in situ* growth system and transferred to other instruments of the PGM beamline, thus allowing extensive film preparation and characterization. A manipulator dedicated to specimen preparation and organic-film deposition with temperature control between 200 K and ~800 K has been developed. The design and performance of the system are reported with emphasis on a novel solution of masks developed to achieve position-dependent film deposition. To demonstrate the enhanced capabilities of the PGM beamline in the growth and in the characterization of electronic-structure studies of organic molecular films and their heterostructures through synchrotron-based spectroscopies, this paper presents some preliminary results of a study of Fe-phthalocyanine growth on Si substrates and on *in situ* prepared $La_{0.67}Sr_{0.33}MnO_3$ buffer layers on $SrTiO_3$ single crystal.

1. Introduction

Organic materials have a broad range of potential applications which include optoelectronic devices, chemical sensors, coatings, *etc.* (Forrest, 1997). They can arrange in rich and complex structures and in many cases they self-assemble on metal surfaces as in the case of planar aromatic compounds such as pentacene derivatives and phthalocyanines grown by organic molecular-beam epitaxy (Forrest, 1997). Although some organic thin films are stable in air and can be measured *ex situ*, clearly experimental apparatus for combined thin-film synthesis and *in situ* characterization is desirable.

The increasing interest in hybrid organic multistructures for spintronic, solar-cell and electronic applications (Reineke *et al.*, 2013) has driven the spread of versatile organic molecular-deposition systems that can be readily coupled with a characterization setup (Ritley *et al.*, 2001).

In particular, the study of the formation of sharp and uncontaminated hybrid organic–inorganic interfaces requires deposition under ultrahigh vacuum (UHV). However, the volatility of some molecules, such as copper(II) 4,4′,4″,4‴-tetraaza-29H,31H-phthalocyanine, BDTDA [4,4′-bis(1,2,3,5-dithiadiazolyl)] among others, in an UHV environment along with a small degree of impurities of heavy-mass organic elements during evaporation (Lewis & Shaffer, 1924) result in an increased base pressure in the chamber. In many cases a modular UHV deposition unit is preferred to the insertion of
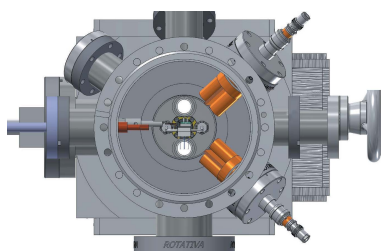
a molecular evaporator on a standard sample-preparation chamber in order to avoid contamination.

Here we report on the latest organic-deposition setup that has been developed at the U11-PGM beamline, LNLS synchrotron, Campinas, Brazil (Cezar *et al.*, 2013). This unit was added to a pre-existing beamline with surface-science facility preparation chambers for the deposition of thin oxide films through the pulsed laser deposition (PLD) method (KrF excimer laser, wavelength of 248 nm) or thin metal films using molecular-beam epitaxy (MBE). The capability of producing organic molecular films and their heterostructures in addition to the oxide–metal and metal–oxide multistructures was achieved in the present work.

The beamline is equipped with a full set of surface-sensitive characterization techniques such as low-energy electron diffraction, an Auger spectrometer, a scanning–tunnelling microscope and others that make use of synchrotron radiation, like UV and X-ray photoelectron spectroscopy (XPS) analyzers, and an X-ray absorption spectroscopy (XAS) detection system in the absence or presence of an applied magnetic field (X-ray magnetic circular dichrosim). Fig. 1 reproduces part of the end station of the PGM beamline: the sample-preparation and characterization UHV chambers. In Fig. 1, the position of the organic molecular beam deposition (OMBE) chamber is shown as well as the incoming synchrotron beam position in the angle-resolved photoemission (ARPES) chamber. The PGM beamline is a prototype surface-science laboratory that is similar to others already present worldwide (Panaccione *et al.*, 2009; Lee *et al.*, 2016; Cantelli *et al.*, 2015).

The OMBE was equipped with Knudsen-style effusion cells for organic-film growth, a quartz crystal-thickness monitor and substrate heating/cooling capabilities. The novelty of the system is the homemade UHV-compatible manipulator that allows sample preparation and a position-dependent film deposition. The organic-molecule UHV chamber can be used independently to grow molecular films or connect to the *in situ* thin-film growth and characterization system available at the PGM beamline. This enables a detailed synthesis and characterization of samples, including synchrotron-based X-ray spectroscopies.

We successfully tested the homemade system during preliminary XPS and XAS characterization of a Fe-phthalocyanine (FePc) film on an SiO_x/Si substrate. Furthermore, we produced and characterized the organic molecule/oxide heterostructures of FePc that were grown on $La_{0.67}Sr_{0.33}MnO_3$ (LSMO) buffer layers on $SrTiO_3$ (STO) substrates. In the latter example, the important role of position-dependent deposition is highlighted.

2. Description of the molecular UHV chamber

Figs. 2(*a*) and 2(*b*) show the three-dimensional design and a photograph of the molecular chamber that comprises the UHV transfer units (manipulator, magnetic transfer rod, wobble stick), the main chamber body with a variety of ports for the evaporation sources and view ports, and the pumping system at the bottom. To make the system as versatile and portable as possible, it is located on a steel frame equipped with wheels for easy displacement of the system. To maintain the vacuum during each step of the experiment, the chamber is individually pumped with a $300 \, l \, s^{-1}$ turbomolecular pump. A base pressure of the order of 10^{-10} mbar is readily achievable after baking the system at 150°C.

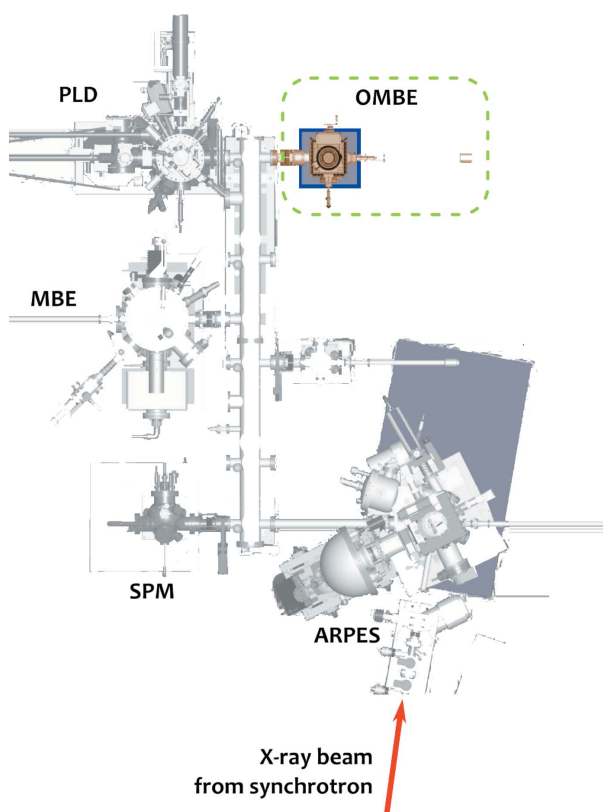A pre-existing UHV chamber was adapted to achieve the best conditions for organic-molecule deposition. It consists of

Figure 1
Layout of the surface-science preparation and characterization facility at the PGM beamline. Each UHV chamber (PLD, MBE, SPM and ARPES) is labelled in the drawing. The position of the organic molecular beam epitaxy chamber is highlighted.
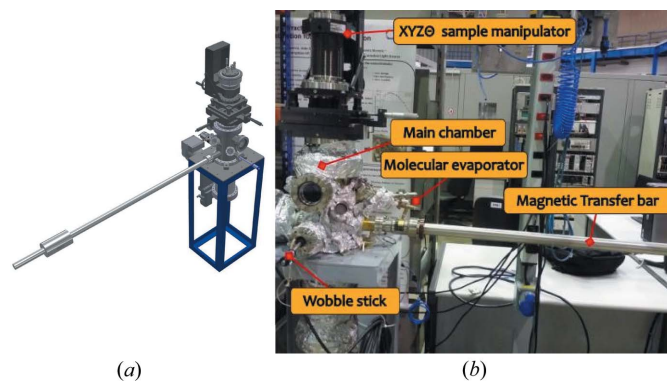

Figure 2
(*a*) Three-dimensional illustration of the UHV molecular chamber. (*b*) Photograph of the molecular chamber. The principal components of the system are highlighted: the *xyz* sample manipulator, the magnetic transfer bar, the molecular evaporators and the wobble stick.
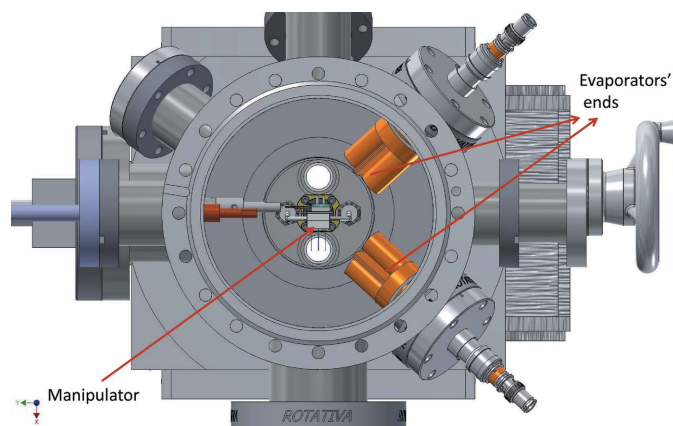
Figure 3
The bottom view of a section of the molecular chamber that shows the relative position of the manipulator and evaporator sources.

Figure 4
Three-dimensional drawing of the UHV manipulator. The characteristic features of the manipulator are indicated: nitrogen cooling reservoir, deposition mask, heaters for sample preparation and temperature control.

two CF200 ports for the pumps and manipulator; one flange CF63 docked to the transfer-unit chamber of the PGM surface-facility system; CF40 ports for the magnetic-transfer rod and a wobble stick; three viewports (CF40 and CF63) used during sample transfer and deposition; and three CF40 ports for molecules and metal evaporators. Two of the ports hosting the molecule evaporators are tilted by 20° from the horizontal to avoid the loss of evaporant loaded in the crucibles; one CF16 port is thought to be used to connect a leak valve that acts as a gas inlet.

We equipped the molecular UHV chamber with a commercial Creaphys evaporator, model DE-DUAL-0.5-CF40-SHMA, which can be loaded with two crucibles. The temperature of each crucible is separately controlled, so it is possible to use each one independently. This enables the deposition or co-deposition of different molecules. We prepared a homemade molecular evaporator based on a Ta filament wrapped around a quartz crucible. The temperature of the crucible is measured using a thermocouple positioned at the exit of the crucible.

The sample–evaporator distance was chosen to be ∼5 cm in order to optimize the deposition time and efficiency. The experimental geometry for the evaporation is highlighted in Fig. 3, where a three-dimensional scheme of the chamber, manipulator and evaporators is shown.

3. Description of the manipulator

The manipulator consists of: (i) two sample stages for standard flag-style sample holders on the same side of the manipulator at two different heights; (ii) an integrated and *in situ* exchangeable quartz microbalance to estimate the evaporation rate; (iii) a water or liquid-nitrogen cooling system used to keep the temperature of both the sample holder and quartz microbalance stable during deposition; (iv) a set of masks for position-selective deposition.

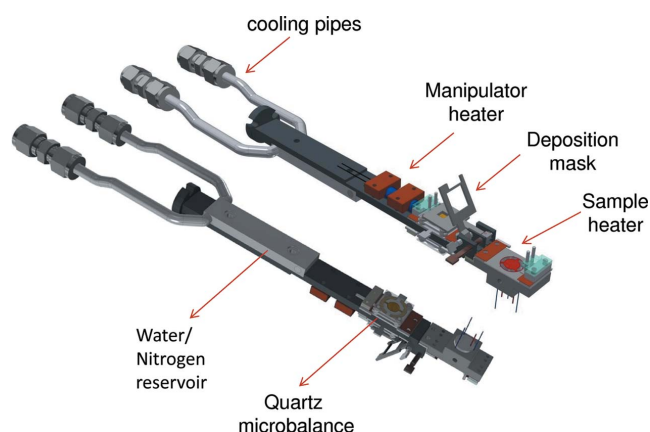In (i), the top sample stage is used for cooling down the sample and for the position-dependent deposition, whereas the bottom sample stage can be used to heat up the substrate. Fig. 4 shows the details of the manipulator.

To achieve substrate temperatures below 300 K, a liquid-nitrogen feed-through, which includes a small reservoir to act as a cryo-shroud, has been installed on the manipulator (as indicated in Fig. 4). The thermal conductivity is improved by an indium contact between the reservoir and copper–oxygen free manipulator head. A heater is installed in the upper part of the manipulator to guarantee a fine temperature control. The lowest temperature reached using liquid nitrogen was ∼200 K. Thermal stabilization of the sample and quartz microbalance during the deposition was obtained by flowing water in the cooling circuit.

A maximum substrate temperature of ∼800 K can be achieved on the bottom sample stage where a ceramic heater from Wavelabs is mounted (Fig. 4). The resistor is fixed to a stainless-steel block that is separated from the copper–oxygen free head with a 1.5 mm-thick ceramic spacer to improve the thermal insulation. The resistive ceramic heater is a good option for substrate thermal treatment in the presence of partial oxygen pressure, essential in the case of thin-film oxide growth. The heater can be used for substrate treatment as well as for depositions that require substrate temperatures above 300 K. The temperatures at the two sample stages are independently measured through thermocouples.

A quartz crystal-thickness monitor is mounted on an adapted flag sample holder according to the solution proposed in by Stavale *et al.* (2008) and shown in Figs. 5(*a*)–5(*b*). The sensor is capable of monitoring the mass density of material deposited with submonolayer resolution, and is useful for estimating molecular-film thicknesses. Owing to the short microbalance-to-evaporator distance in the OMBE chamber, the thermal load on the quartz crystal is too high, preventing a reliable thickness-rate reading using the design by Stavale *et al.* (2008). We had to modify the original design and improve the thermal contact between sensor holder and manipulator to permit the water cooling system to stabilize the microbalance temperature. The quartz balance is hosted at the back of the
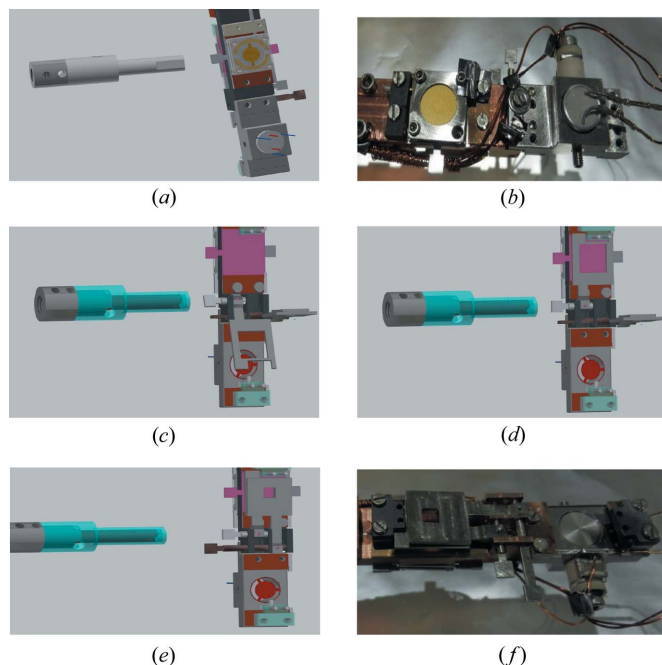
Figure 5
(a)–(b) Sketches and photographs of the side of the manipulator that hosts the quartz microbalance; (c)–(f) sketches and photographs of the manipulator (c) without the use of a mask, (d) with the use of a 10 mm × 10 mm mask and (e)–(f) with the use of a 5 mm × 5 mm mask. The relative position of the masks can be varied by using the same wobble stick implemented in the sample transfer.

upper sample stage. After the deposition-rate calibration, one need only rotate the manipulator by 180°.

One of the sample stages is equipped with a set of masks to limit the region of the substrate that receives the deposition. The distance between sample and mask is ∼2 mm, optimized to have the possibility to introduce a sample with a different thickness. This parameter and the angle at which the evaporators are mounted may affect the shadow on the deposition. The lateral precision, *i.e.* the definition of two adjacent regions of different thicknesses, in the actual set-up is estimated to be around 0.5 mm, but it can be improved by refining the design and piece realization. Figs. 5(c)–5(f) shows the operational principle of the masks. The sample can be exposed to the evaporation either without any mask (shown in Fig. 5c), with a mask of 10 mm × 10 mm (Fig. 5d) or with a mask of 5 mm × 5 mm (Figs. 5e–5f). The masks are moved from open to closed positions by the same wobble stick used for the sample transfer through levers that have the same square termination of sample-holder plates. The largest mask was designed in such a way that it can be fitted with an additional patterned mask. This feature can be used, for example, to deposit electrodes pads on the film for transport measurements.

4. Results and discussion

Self-assembled metal phthalocyanine thin films are receiving considerable interest because of their potential technological applications. An important issue is the growth of this thin
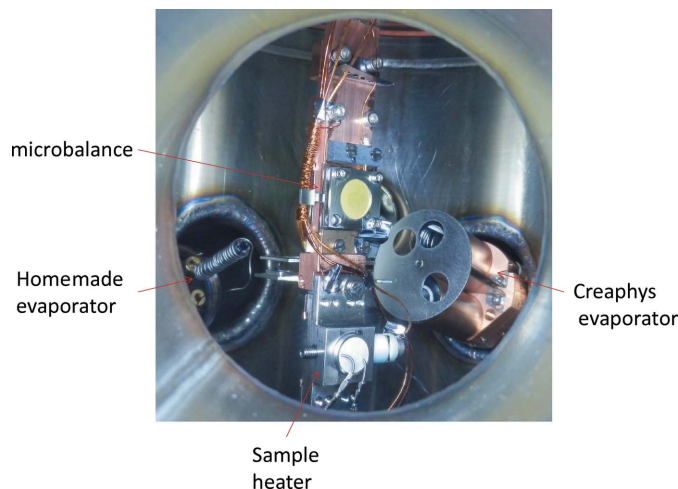

Figure 6
The experimental setup during molecular deposition: the sample on the manipulator faces of the homemade molecule evaporator. The represented case does not make use of masks, *i.e.* the case depicted in Fig. 5 (c).

molecular film on technologically relevant substrates such as SiO_x/Si. In fact, owing to their thermal stability at elevated temperatures, these molecules have been explored for their application in organic field-effect transistors and solar cells on silicon-based supports (Abhishek *et al.*, 2018).

SiO_x/Si was introduced under vacuum and no further treatment was perfomed before FePc deposition.

Fig. 6 shows the evaporation geometry where the sample is facing a homemade FePc evaporator. For reference, the quartz crucible is inside the Ta heating coil seen on the left-hand side of the photograph. One can notice that both masks are open. On the right-hand side of the picture, one can notice the tip of the double commercial evaporator not used for these results.

Before the evaporation, we estimated the FePc evaporation rate to be 0.6 Å min^{-1} using the quartz microbalance mounted on the manipulator. The substrate was exposed to FePc evaporator for 20 min.

The sample was transferred *in situ* to the ARPES chamber where it was characterized by XPS and XAS. The photoelectron spectra were measured at 520 eV on an FePc(1.5 nm)/SiO_x/Si(111) interface (Fig. 7). The photon energy was selected in order to maximize both N 1s and C 1s core-evel cross-sections, both features visible in the long energy range spectrum. In the present example, the C 1s core-level spectrum is given by the superposition of two contributions: two C sites of an FePc molecule and atmospheric C contamination for a substrate without surface preparation. Therefore, we highlighted the N 1s contribution, a clear fingerprint of the FePc film (inset of Fig. 7) (Annese *et al.*, 2015). In Fig. 8 we show Fe $L_{2,3}$ and N K XAS spectra of the FePc film on an SiO_x/Si substrate at a grazing incidence of 55.4°. We observed the typical spectra of a thick FePc film, which indicated the weak interactions between the molecule and the underlying surface (Annese *et al.*, 2015).

LSMO thin films are particularly interesting for their unusual electronic structure, magnetic and charge transport properties; they are frequently used as components in multi-
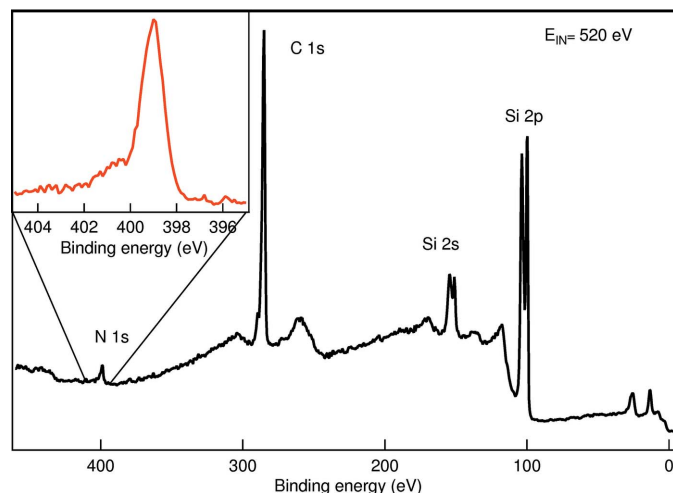
Figure 7
Thin film of FePc grown on an SiO$_x$/Si substrate. N 1s and C 1s core-level features related to the FePc molecule are highlighted in the spectrum. Inset: enlargement of the binding energy around the N 1s peak. The measurement was performed using a photon energy of 520 eV at the PGM beamline with the sample kept at room temperature.
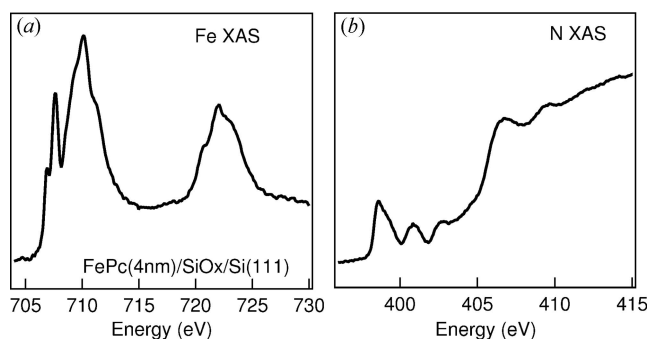

Figure 8
(a) Fe $L_{2,3}$ and (b) N K XAS spectra measured on an SiO$_x$/Si substrate at a grazing incidence of 35° from the substrate surface.

the following growth parameters: laser fluence, 1.1 J cm^{-2}; post-annealing oxygen partial pressure, 10^2 mbar; and time, 1 h. The quality of LSMO films was evaluated with XPS and XAS (not shown). The films were transferred *in situ* to the OMBE chamber.

The position-dependent deposition was evaluated by evaporating FePc onto two LSMO thin films, the centers separated by ~4 mm. Two (STO) (100) single crystals (A and B) were mounted on the same sample plate as shown in Fig. 9(a). The heterostructure preparation consisted of the oxide evaporation in PLD and the molecule film growth in the OMBE chamber; its characterization was performed in the ARPES chamber.

FePc film deposition was performed in two steps: (i) both masks open and FePc evaporated on both LSMO films for 8 min (Fig. 6); (ii) both masks closed, only substrate A is exposed to the molecule flux. In the second configuration, the time of exposure to FePc flux was 16 min. The total FePc evaporation time for A and B was 24 min and 8 min, respectively. The FePc deposition rate was fixed at 0.6 Å min^{-1}, thus sample A was ~1.5 nm thick and sample B ~0.5 nm thick.

In Fig. 9(c), we report the Fe $L_{2,3}$ XAS spectra measured on samples A and B at $\theta = 55°$ from the sample normal. The X-ray absorption spectra displayed the typical Fe $L_{2,3}$ line shape for thin and thick FePc films (Bartolomé *et al.*, 2010; Annese *et al.*, 2015). Thus, proper use of the masks allows the user to grow multiple films on the same sample plate. This implies less sample transfers, which can lead to more efficient use of synchrotron beam time.

5. Conclusions

We have designed, built and commissioned a modular UHV system optimized for organic molecules and metal thin-film deposition. The versatility of the homemade manipulator allows deposition within the temperature range 200–800 K and a choice of the sample area to be exposed to evaporation. Moreover, a preliminary calibration of the film thickness was achieved by a thickness sensor hosted in the manipulator. The spectroscopic results relative to thin FePc films on LSMO prepared and characterized *in situ* and on SiO$_x$/Si substrates
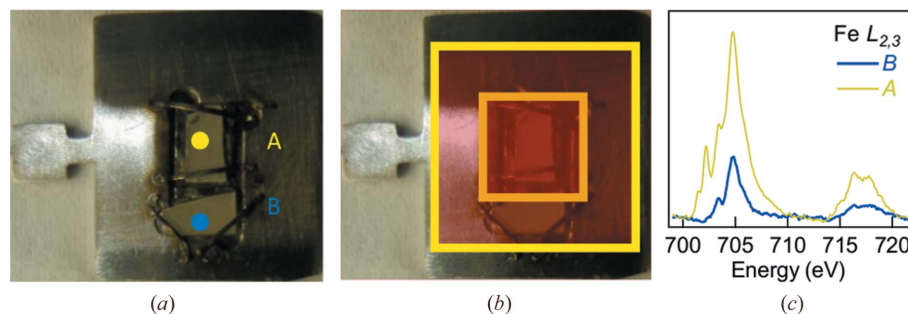
structure spin valves because of their associated high-spin polarization. Lately, LSMO thin films have gained an important role in both inorganic (Majumdar & Dijken, 2014) and hybrid organic–inorganic spintronic applications (Dediu *et al.*, 2009; Naber *et al.*, 2007). In this context, it is important to have the possibility to control the deposition of organic molecules and LSMO thin film in the same specimen-preparation facility. We have already performed a concomitant optimization of LSMO growth by PLD as reported by Annese *et al.* (2018) in order to obtain a thin film with optimal magnetization and a smooth surface morphology.

LSMO films, 60 nm thick, were prepared by the PLD method. The preparation of the oxide film was carried out using the procedure explained by Annese *et al.* (2018), with

Figure 9
(a)–(b) SrTiO$_3$ substrates fixed onto the sample holder before the two subsequent depositions of LSMO (PLD chamber) and FePc (molecular chamber). In panel (b) the position of the two masks is highlighted by a coloured squared box; (c) Fe $L_{2,3}$ XAS spectra measured in the two positions drawn in (a), after molecular deposition on LSMO thin film, keeping the internal mask of 5 mm × 5 mm at a close distance with respect to the specimen.

show optimal operation of the OMBE chamber along with the PGM beamline.

References

Abhishek, K., Denys, N., Luca, C., Luisa, B., Alberto, C. & Maddalena, P. (2018). *J. Raman Spectrosc.* **1**, 8.

Annese, E., Mori, T., Schio, P., Rache Salles, B. & Cezar, J. (2018). *Appl. Surf. Sci.* **437**, 281–286.

Annese, E., Rosi, A., Fujii, J. & Sakamoto, K. (2015). *J. Phys. Chem. C*, **119**, 20065–20073.

Bartolomé, J., Bartolomé, F., García, L. M., Filoti, G., Gredig, T., Colesniuc, C. N., Schuller, I. K. & Cezar, J. C. (2010). *Phys. Rev. B*, **81**, 195405.

Cantelli, V., Geaymond, O., Ulrich, O., Zhou, T., Blanc, N. & Renaud, G. (2015). *J. Synchrotron Rad.* **22**, 688–700.

Cezar, J. C., Fonseca, P. T., Rodrigues, G. L. M. P., de Castro, A. R. B., Neuenschwander, R. T., Rodrigues, F., Meyer, B. C., Ribeiro, L. F. S., Moreira, A. F. A. G., Piton, J. R., Raulik, M. A., Donadio, M. P., Seraphim, R. M., Barbosa, M. A., de Siervo, A., Landers, R. & de Brito, A. N. (2013). *J. Phys. Conf. Ser.* **425**, 072015.

Dediu, V. A., Hueso, L. E., Bergenti, I. & Taliani, C. (2009). *Nat. Mater.* **8**, 707–716.

Forrest, S. R. (1997). *Chem. Rev.* **97**, 1793–1896.

Lee, J. H., Tung, I. C., Chang, S.-H., Bhattacharya, A., Fong, D. D., Freeland, J. W. & Hong, H. (2016). *Rev. Sci. Instrum.* **87**, 013901.

Lewis, H. F. & Shaffer, S. (1924). *Indust. Eng. Chem.* **16**, 717–718.

Majumdar, S. & van Dijken, S. (2014). *J. Phys. D Appl. Phys.* **47**, 034010.

Naber, W. J. M., Faez, S. & van der Wiel, W. G. (2007). *J. Phys. D Appl. Phys.* **40**, R205–R228.

Panaccione, G., Vobornik, I., Fujii, J., Krizmancic, D., Annese, E., Giovanelli, L., Maccherozzi, F., Salvador, F., De Luisa, A., Benedetti, D., Gruden, A., Bertoch, P., Polack, F., Cocco, D., Sostero, G., Diviacco, B., Hochstrasser, M., Maier, U., Pescia, D., Back, C. H., Greber, T., Osterwalder, J., Galaktionov, M., Sancrotti, M. & Rossi, G. (2009). *Rev. Sci. Instrum.* **80**, 043105.

Reineke, S., Thomschke, M., Lüssem, B. & Leo, K. (2013). *Rev. Mod. Phys.* **85**, 1245–1293.

Ritley, K. A., Krause, B., Schreiber, F. & Dosch, H. (2001). *Rev. Sci. Instrum.* **72**, 1453–1457.

Stavale, F., Niehus, H. & Achete, C. A. (2008). *Rev. Sci. Instrum.* **79**, 105102.